

NUMERICAL SIMULATION OF LAMINAR AND TURBULENT FLOWS AROUND RECTANGULAR CYLINDERS

ATSUSHI OKAJIMA, HISANORI UENO AND HARUHISA SAKAI

Department of Mechanical Systems Engineering, Kanazawa University, 2-40-20, Kodatsuno, Kanazawa 920, Japan

SUMMARY

By a finite volume method, laminar flows around bluff bodies with a rectangular cross-section of various width-to-height ratios from 0.2 to 10 and with a cross-section of a round leading edge and a square trailing edge have been computed on body-fitted curvilinear co-ordinates at Reynolds numbers of $(1, 4, 7) \times 10^3$. Turbulent flows have also been computed by a standard $k-\epsilon$ turbulence model. Computed results are compared with experimental data at a Reynolds number of 10^3 and clearly show the effects of the shape of the bluff body on the aerodynamic characteristics. We can successfully simulate some interesting phenomena whereby the flow pattern changes critically when the side ratio B/H is about 2.1 and 6; that is, a fully separated flow, an alternately reattached one and a stationarily reattached one. The results also reveal interactions between the wake and separation bubbles. There are, however, significant discrepancies between the results from the $k-\epsilon$ turbulence model and experiments.

KEY WORDS Numerical simulation Laminar flow Turbulent flow Rectangular cylinder SIMPLE method Separation bubble

1. INTRODUCTION

Unsteady separated flows about bluff bodies such as circular cylinders, rectangular cylinders, flat plates and cylinders with other blunt cross-sections are of direct relevance to many practical applications, e.g. chimneys, steel tower suspension bridges, buildings and other structures. Flows around bluff bodies with a rectangular cross-section in particular have been studied by both experiments and numerical calculations on the aerodynamic and aeroelastic characteristics of the bodies.^{1–6} We have recently reported the existence of a critical range of Reynolds numbers where the flow pattern changes abruptly with a drastic variation in the Strouhal number curves against the Reynolds number.^{2,4–6} Some interesting phenomena whereby flow patterns and aerodynamic characteristics such as drag and lift forces, the base pressure and the Strouhal number for a cylinder with a rectangular cross-section are strongly dependent on the shape of the cross-section and the Reynolds number were found by experiments.^{2,3,5} Thus in the present paper we have simulated laminar and turbulent flows about different cylinders with a rectangular cross-section of various width-to-height ratios from 0.2 to 10, which have a leading edge of a round semicircular section or a square section, by the finite difference method at Reynolds numbers of $(1, 4, 7) \times 10^3$. Computed results are compared with experimental data at a Reynolds number of 10^3 . We can thus get a great deal of information about the effects of the shape of the model and gain better insight into the fluid characteristics about bluff bodies with various cross-sections. It is

also expected that the results⁵ previously measured can be confirmed and further reasonably interpreted by comparison with the corresponding computed ones.

2. OUTLINE OF NUMERICAL SIMULATION

First, laminar flows assumed to be two-dimensional, unsteady, incompressible and viscous have been computed in terms of the primitive variables, i.e. velocities and pressure. The fundamental equations are the continuity equation and the Navier–Stokes equations and the pressure is solved to satisfy the continuity equation by the Poisson equation for pressure, following the SIMPLE method. Then we have computed turbulent flows also utilizing the standard k – ε turbulence model. The governing equations of the continuity equation and the Navier–Stokes equations are integrated over elementary control volumes on a body-fitted curvilinear co-ordinate system, i.e. the finite control volume method is employed here. The QUICK upwind difference scheme is applied for the approximation of the convective terms, while all other terms are approximated by second-order central differencing. Then, for time marching, the Navier–Stokes equations discretized by the finite difference schemes on modified staggered meshes are solved by the Crank–Nicolson scheme, which is implicit, and the Poisson equation for pressure is solved by the successive overrelaxation (SOR) method. As for boundary conditions, the flow is undisturbed and uniform at the upstream inlet, while the flow conditions at the downstream exit are given by the use of zero-gradient boundary conditions. For the case of laminar flows the condition of no slip is imposed on the solid surfaces. In the turbulent flow case the generalized logarithmic law is employed to estimate the wall shear stresses on the solid surfaces. For other details of this computation the reader is referred to References 4 and 6. Figure 1 shows the modified O-type grids for the computation of flow around a body.

3. COMPUTED RESULTS

Laminar flows around bluff bodies with a rectangular cross-section of various width-to-height ratios from 0.2 to 10 have been computed, and for the two cylinders with side ratios of 0.6 and 2 turbulent flows have also been simulated by the standard k – ε turbulence model. Some typical results are presented here. Figures 2–13 show streamlines, streak lines or time lines and equivorticity lines which visualize and describe the flows in different ways, and the time-dependent evolutions of the drag (C_D) and lift (C_L) coefficients of the cylinders are also presented in these figures.

3.1. The $B/H=0.2$ cylinder

Figures 2(a) and 2(b) show the flow pattern and equivorticity contour lines respectively around the cylinder with $B/H=0.2$, the thinnest in the present computations at $Re=10^3$. These figures pertain to the instant of upward maximum lift force on the rectangular cylinder and a distinct vortex street is formed in a regular arrangement. Figures 2(c) and 2(d) present plots of computed instantaneous C_D and C_L against time respectively, both of which have high periodicity. It is noted that the values of the mean drag and the amplitude of the lift are smaller than those on the $B/H=0.6$ cylinder.

3.2. The $B/H=0.6$ cylinder

Figures 3(a), 3(b), 4(a) and 4(b) show the laminar ($Re=10^3$) and turbulent flow patterns and equivorticity contour lines respectively about the cylinder with $B/H=0.6$, which is well known to

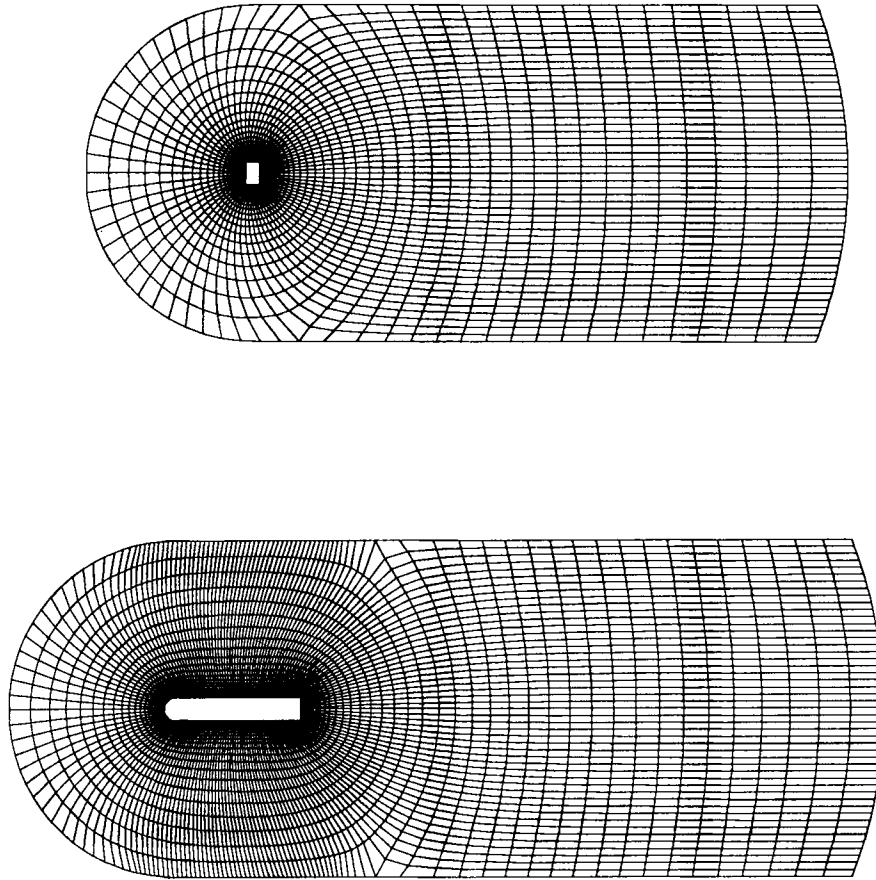


Figure 1. The modified O-type grids for flows around the $B/H = 0.6$ cylinder (top) and the $B/H = 6$ cylinder with a round leading edge (bottom)

undergo the biggest drag force.^{1,2} Figures 3(c), 3(d), 4(c) and 4(d) show the corresponding time evolutions of drag and lift on this cylinder. From a time of about 30–50 after an impulsive start, the cylinder experiences the largest force of time-averaged drag ($C_D = 2.5$) in the present computations and the lift force in both laminar and turbulent flows fluctuates with a large amplitude as a strong vortex street grows in a regular arrangement.

3.3. The $B/H = 1$ cylinder

The flow pattern for the $B/H = 1$ cylinder at $Re = 10^3$ (Figure 5) demonstrates that the vortex street become arranged in a relatively wide wake and that the separated shear flow tends more frequently to interact with the trailing edge than in the cases of the $B/H = 0.4$ and 0.6 cylinders. The appearance of the subharmonic in the C_L -curve (Figure 5(d)) signifies modulations in shedding frequency.

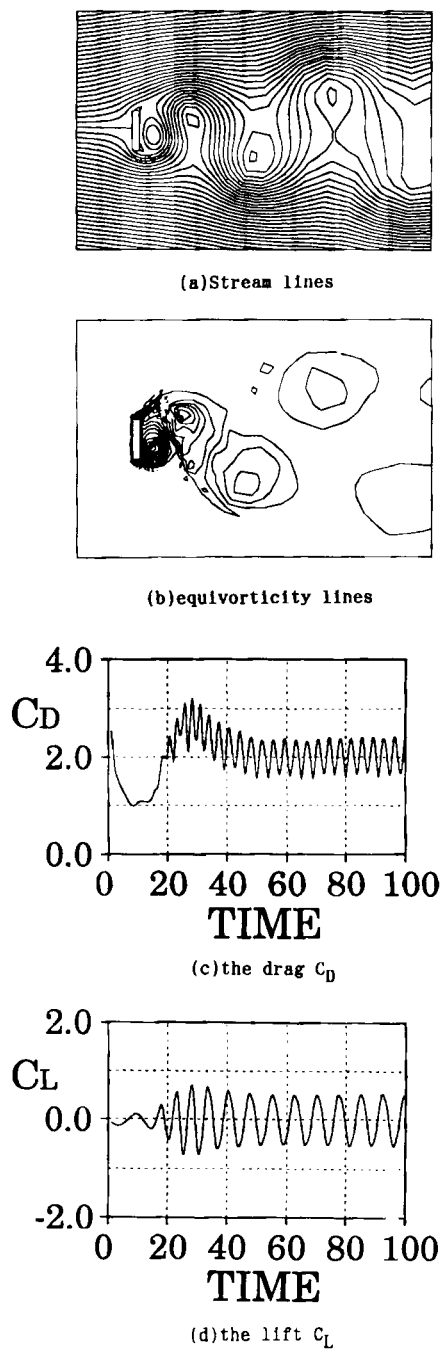


Figure 2. The $B/H=0.2$ cylinder ($Re=10^3$, direct method).

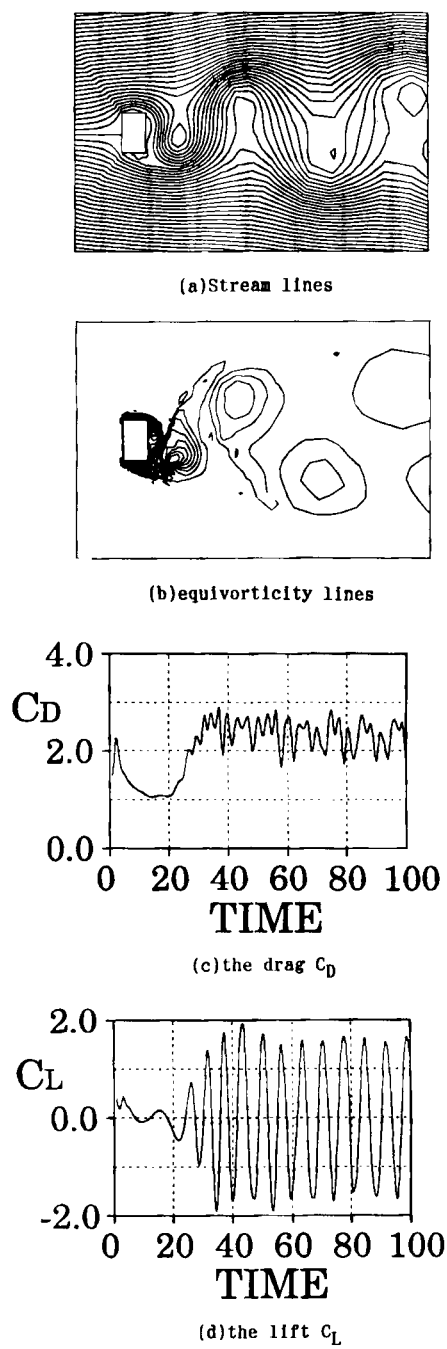
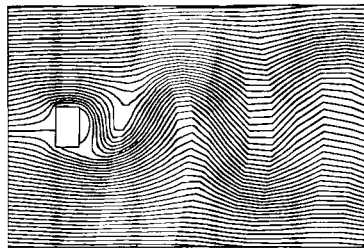
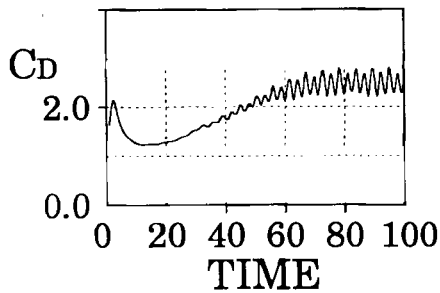
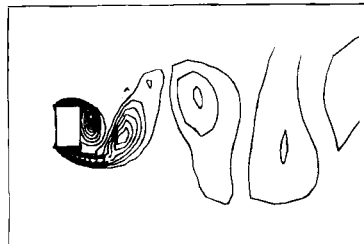


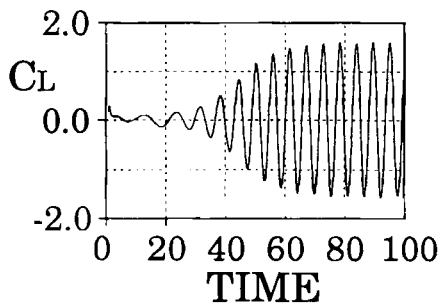
Figure 3. The $B/H=0.6$ cylinder ($Re=10^3$, direct method).



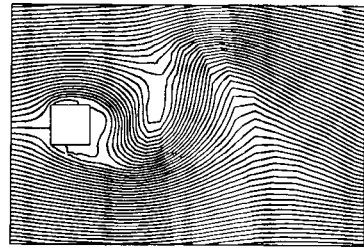
(a)Stream lines



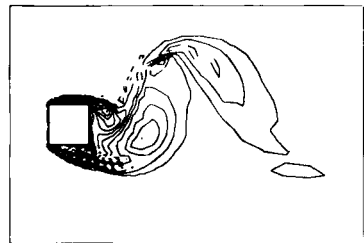
(c)the drag C_D



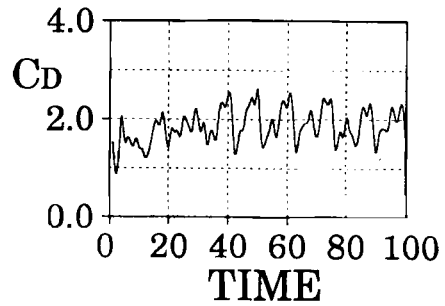
(d)the lift C_L



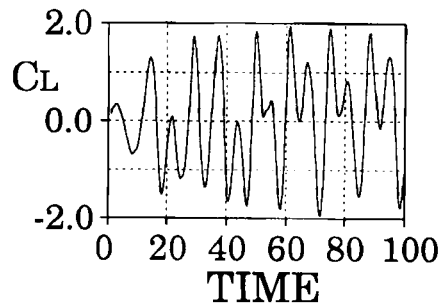
(a)Stream lines



(b)equivorticity lines



(c)the drag C_D



(d)the lift C_L

Figure 4. The $B/H = 0.6$ cylinder ($k-\epsilon$ turbulence model)

Figure 5. The $B/H = 1$ cylinder ($Re = 10^3$, direct method)

3.4. The $B/H=2$ cylinder

Figures 6 and 7 show the laminar ($Re=10^3$) and turbulent flows respectively for the $B/H=2$ cylinder. The separated shear layers keep on detaching from the cylinder, which results in the formation of a large-sized vortex street with lower Strouhal frequency, as shown in Figure 6, when the flow is assumed to be laminar. The laminar flows around the cylinders with side ratios less than about 2:1 can be successfully predicted to have a large time-averaged recirculation zone. On the other hand, the $k-\varepsilon$ turbulence model failed to predict a fully separated pattern around this cylinder, as shown in Figure 7. The profiles in the near field and the pattern of the wake vortex street are poorly predicted as compared with the experiments;² that is, the flow pattern computed with the $k-\varepsilon$ turbulence model has a very narrow wake and the shear layers separated from the leading edges flow down along the side surfaces, like a flow at very low Reynolds number.

3.5. The $B/H=3$ and 4 cylinders

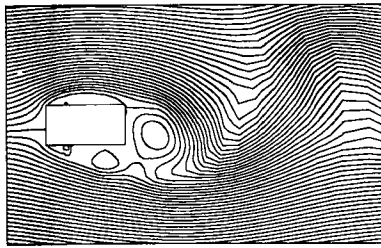
The flow around the $B/H=3$ cylinder alternately reattaches on the side surfaces, accompanied by an instantaneous formation of separation bubbles on the side surfaces, as shown in Figures 8(a) and 8(b). The periodic character of the flow around the cylinder is well predicted. The plots of the lift coefficient C_L of this cylinder have a constant amplitude with high periodicity, as shown in Figure 8(d). We cannot, however, obtain the flow pattern modulated with a subharmonic Strouhal component about this cylinder as measured by the experiments,² while a subharmonic Strouhal component appears for the $B/H=2:1$ cylinder (see Figure 14(b)). For the $B/H=4$ cylinder the separated flows reattach onto the cylinder surfaces and their motion synchronizes with the Strouhal frequency of the wake, as shown in Figure 9. The computed patterns are proven to closely resemble the visualized patterns.⁵ The reattachment points about the $B/H=3$ and 4 cylinders are never stationary, being alternately swept away downstream, although the time-averaged positions of these points can be ascertained to stay on the side surfaces. It can be seen that the vortex street in Figures 8 and 9 is more regularly shaped and less stretched than that for the $B/H=2$ cylinder in Figure 6.

3.6. The $B/H=6$ cylinder

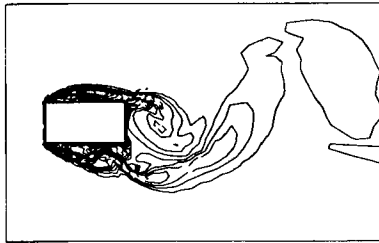
The separated shear layer becomes more frequently interfered with by the after-body of an elongated cylinder. Figures 10(a)~10(d) show the laminar flow configuration and the time evolution of fluid forces respectively for the $B/H=6$ cylinder. We can also see in these figures that some small vortices are generated and shed downstream owing to instability of the separated shear layers. It can also be proven that the separated shear layer reattaches not steadily but alternately on the surfaces and that some vortices flow downstream along the surfaces into a wake vortex street, linking with the unsteady motion of separation bubbles. The time variation of C_L is modulated in Figure 10(d) and two components of the Strouhal number appear in the spectrum of C_L which are mainly affected by the fluctuation of pressure on the surfaces. It is noteworthy that the higher component is predominant in the power spectrum of the velocity fluctuation in the wake.

3.7. The $B/H=8$ cylinder

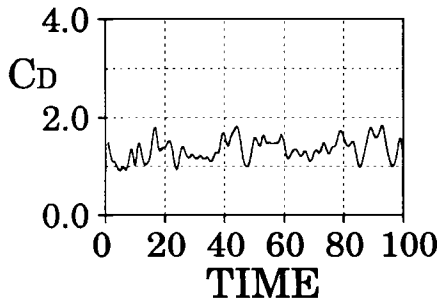
As for the cylinder with long side surfaces, the separated shear layer is easily reattached onto the upper and lower surfaces, followed by shedding of a narrow vortex street downstream behind the base surface, as shown in Figure 11. Therefore the component with high Strouhal number induced by the wake becomes distinguished in the power spectrum of the lift force.



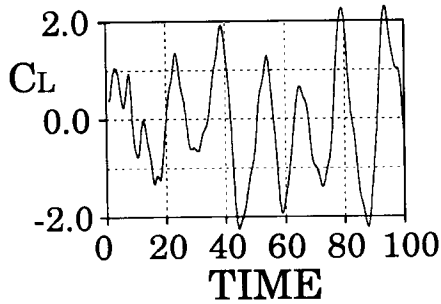
(a)Stream lines



(b)equiporticity lines

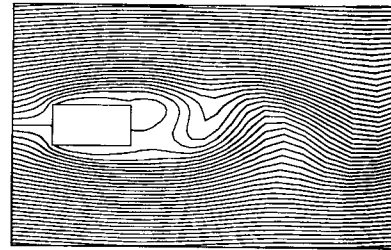


(c)the drag C_D

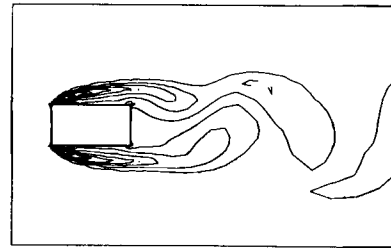


(d)the lift C_L

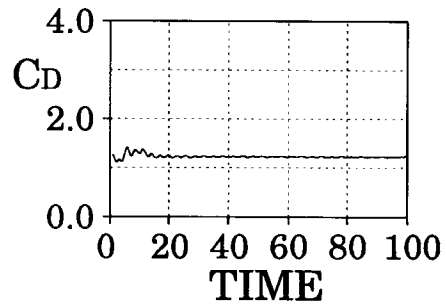
Figure 6. The $B/H=2$ cylinder ($Re=10^3$, direct method)



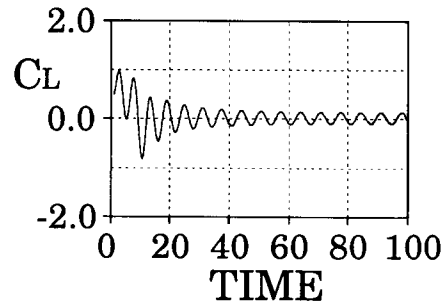
(a)Stream lines



(b)equiporticity lines

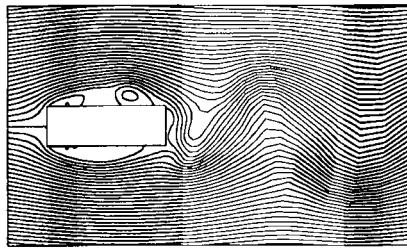


(c)the drag C_D

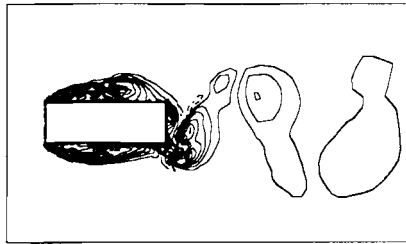


(d)the lift C_L

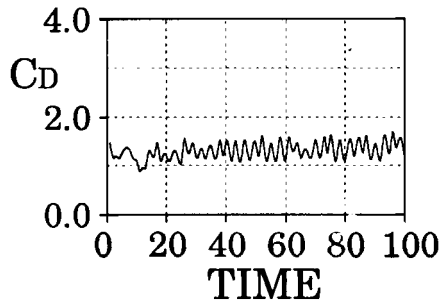
Figure 7. The $B/H=2$ cylinder ($k-\epsilon$ turbulent model)



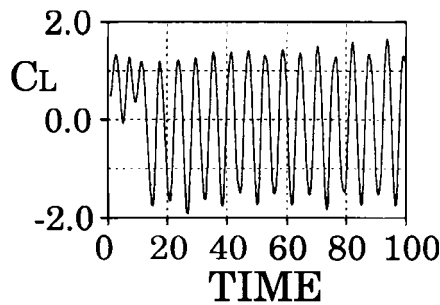
(a)Stream lines



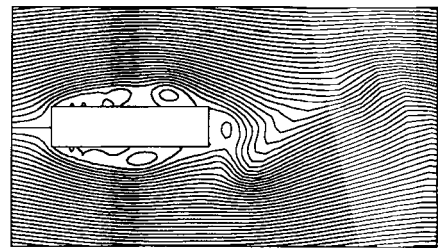
(b)equivorticity lines



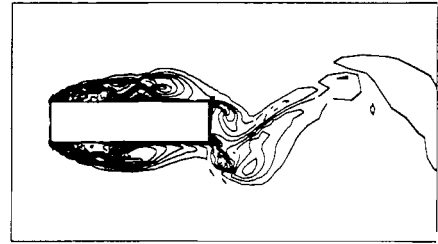
(c)the drag C_D



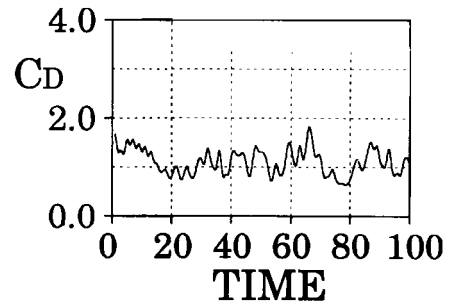
(d)the lift C_L



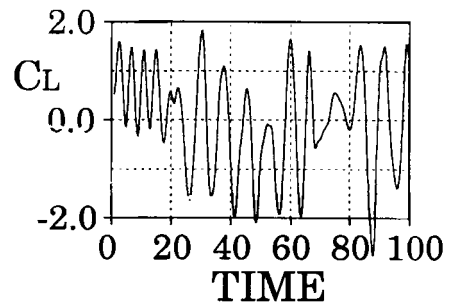
(a)Stream lines



(b)equivorticity lines



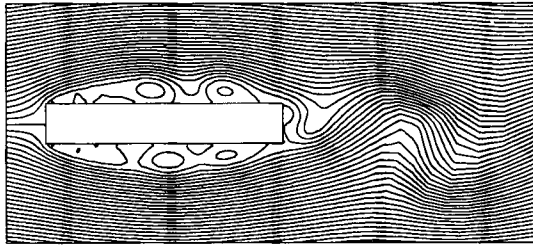
(c)the drag C_D



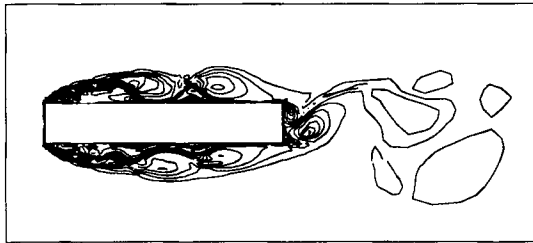
(d)the lift C_L

Figure 8. The $B/H=3$ cylinder ($Re=10^3$, direct method)

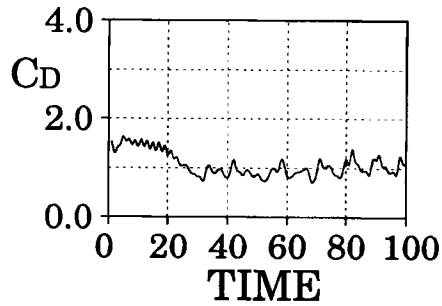
Figure 9. The $B/H=4$ cylinder ($Re=10^3$ direct method)



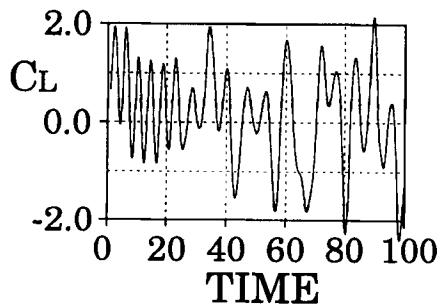
(a)Stream lines



(b)equivorticity lines

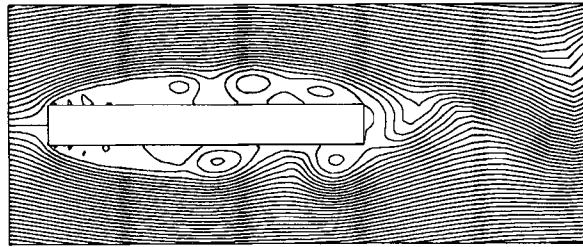


(c)the drag C_D

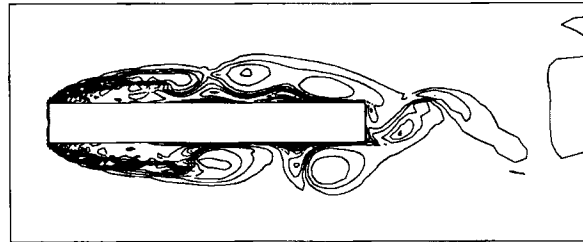


(d)the lift C_L

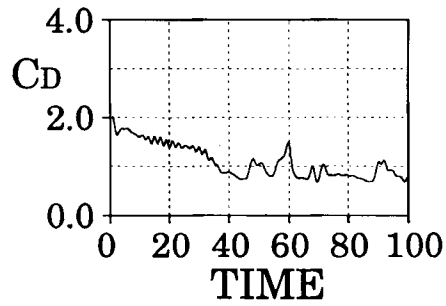
Figure 10. The $B/H=6$ cylinder ($Re=10^3$, direct method)



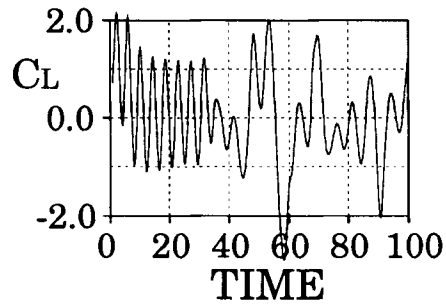
(a)Stream lines



(b)equivorticity lines

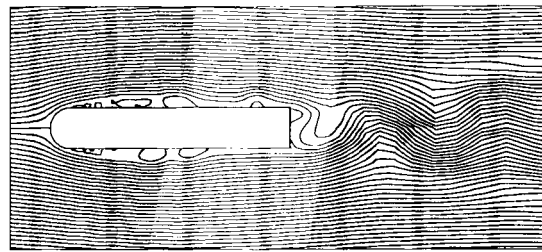


(c)the drag C_D

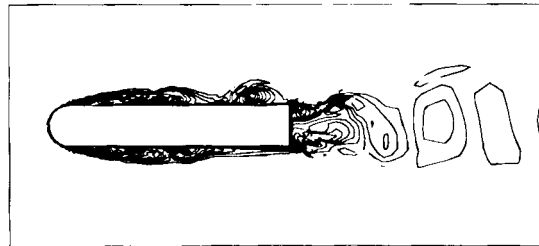


(d)the lift C_L

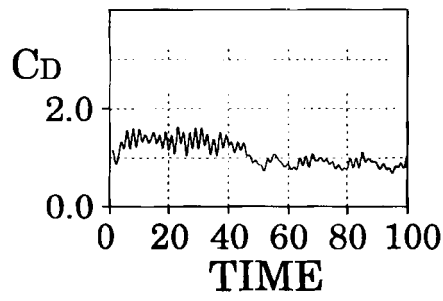
Figure 11. The $B/H=8$ cylinder ($Re=10^3$, direct method)



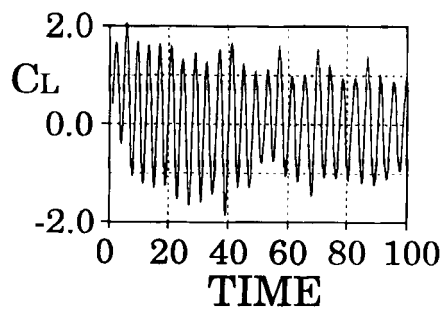
(a)Stream lines



(b)equivorticity lines

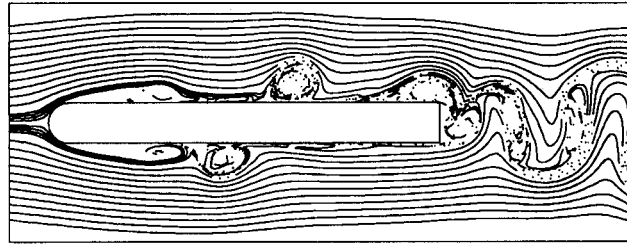


(c)the drag C_D

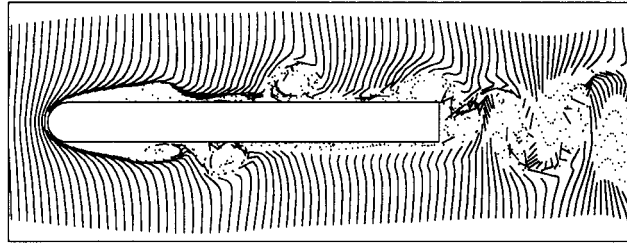


(d)the lift C_L

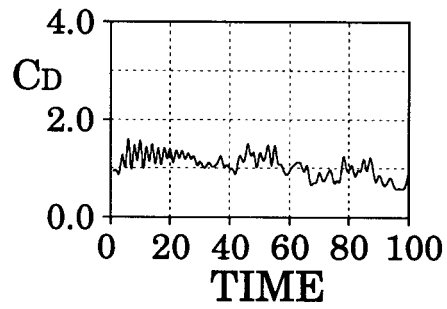
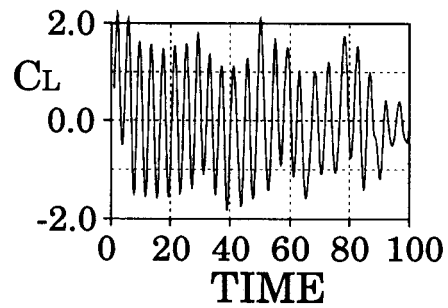
Figure 12. The $B/H=6$ cylinder with a round leading edge ($Re=4 \times 10^3$, direct method)



(a)streak lines



(b)time lines

(c)the drag C_D (d)the lift C_L Figure 13. The $B/H=10$ cylinder with a round leading edge ($Re=7 \times 10^3$, direct method)

3.8. The $B/H=6$ and 10 cylinders with a round leading edge

We make the leading edges of an elongated cylinder round (semicircular) in order to reduce the size of separation bubbles formed near the leading edges and to examine how the vortex street is arranged behind the base surface, linking with the unsteady motion of separation bubbles. It is certified that the separated shear layers can impinge and be easily reattached onto the upper or lower surface, followed by shedding of a narrow vortex street downstream, as shown in the streamlines, the equivorticity lines, the streak lines and the time lines of Figures 12 ($Re=4 \times 10^3$) and 13 ($Re=7 \times 10^3$), and that the separation bubbles shrink and the vortex street is shed from the trailing edges, regularly arranged in the wake.

3.9. Comparison between the computed and experimental results

The computed results of the mean drag coefficient \bar{C}_D and the mean base pressure $-\bar{C}_{pb}$, and the Strouhal number St of the velocity fluctuation in the wake and at the trailing edges, are

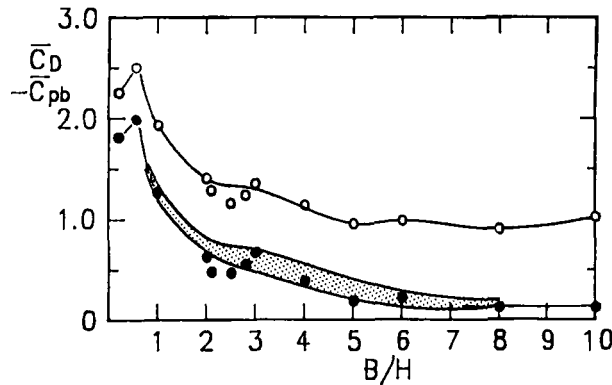


Figure 14(a). Comparison between the computed and experimental results of \bar{C}_D and $-\bar{C}_{pb}$ at $Re=10^3$: \circ , computed \bar{C}_D ; \bullet , computed $-\bar{C}_{pb}$; \otimes , experimental $-\bar{C}_{pb}$

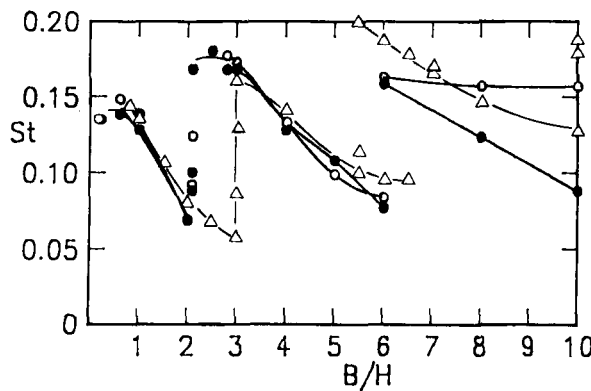


Figure 14(b). Comparison between the computed and experimental results of St at $Re=10^3$: \circ , computed St in wake; Δ , experimental St in wake; \bullet , computed St at trailing edge

summarized against the side ratio B/H of the cylinder in Figures 14(a) and 14(b), compared with the experimental values of base pressure and Strouhal number^{4,5} at $Re = 10^3$. In this figure the computed values of both \bar{C}_D and $-\bar{C}_{pb}$ reach a maximum when the side ratio B/H is about 0.6, and the computed values of $-\bar{C}_{pb}$ are within a scatter of the experimental data shown by the shaded area, indicating satisfactory agreement between them. Critical values of the side ratio of about $B/H = 2.1$ and 6 are clearly found to exist for the computed curve of Strouhal number versus B/H ratio, though the value $B/H = 2.1$ is slightly smaller than the value of 2.8 which is obtained by experiments^{2,5} at $Re = 10^3 - 10^4$.

3.10. Change of computed flow pattern with the side ratio

We have succeeded in the simulation of the change of flow near the critical values of the side ratio, $B/H = 2.1$ and 6. For a rectangular cylinder with a side ratio less than about 2.1 the flow is fully separated from the cylinder, oscillating with a low Strouhal number. Then the flow pattern changes to an alternately reattached flow with a high Strouhal number when the side ratio is beyond about 2.1, owing to the effect of an elongated after-body. For a side ratio from 2.1 to 6, separated shear flows alternately reattach on the surfaces during each period of vortex shedding. Then, on the long side surfaces of a cylinder with $B/H > 6$, separated shear layers impinge on the surface, shedding a vortex street downstream; in the time-averaged pattern, however, the closed separation bubbles remain on the surfaces. With an increase in B/H ratio, the motion of the bubbles is gradually suppressed and a vortex street is more actively shed with a high Strouhal number just behind the base surface.

4. CONCLUSIONS

Laminar and turbulent flows about rectangular cylinders with B/H ratios from 0.2 to 10 were simulated by the finite volume method and also utilizing the $k-\epsilon$ turbulence model. The computed laminar flow results compare well with the experiments and successfully reveal the effects of the shape of bluff bodies on the aerodynamic characteristics at a Reynolds number of 10^3 . The wake vortex street can be simulated linking with the motion of separation bubbles at $Re = (1, 4, 7) \times 10^3$. There are, however, discrepancies between the results from the computations by the $k-\epsilon$ model and the experiments.

REFERENCES

1. H. Nakaguti, K. Hashimoto and S. Muto, 'An experimental study of aerodynamic drag of rectangular cylinders', *J. Jpn. Soc. Aero. Space Sci.*, **16**, (168), 1-5 (1968) (in Japanese).
2. A. Okajima, 'Strouhal number of rectangular cylinder', *J. Fluid Mech.*, **123**, 379-398 (1982).
3. R. Parker and M. C. Welsh, 'Effects of sound on flow separation from blunt flat plates', *Int. J. Heat Fluid Flow*, **4**, (2), 113-127 (1983).
4. A. Okajima, T. Nagahisa and A. Rokugou, 'A numerical analysis of flow around rectangular cylinders', *Jpn. Soc. Mech. Eng. Int. J., Ser. II*, **33**, (4), 702-711 (1990).
5. A. Okajima, 'Change of flow about an elongated rectangular cylinder in a range of Reynolds numbers of 200 to 0.7×10^4 ', Paper in *FED Forum on Turbulent Flows, Am. Soc. Mech. Eng.*, **112**, 107-113 (1991).
6. A. Okajima, 'Numerical simulation of flow around rectangular cylinder', *J. Wind Eng. Ind. Aerodyn.*, **33**, 171-180 (1990).